Friction-driven Three-foot Robot Inspired by Snail Movement

Tianqi Yue[1], Hermes Bloomfield-Gadêlha[1] and Jonathan Rossiter[1]

***Abstract*— Snails have amazing adhesive locomotion abilities which help them climb up walls and even across ceilings. They generate this versatile and stable movement by muscular exploiting travelling waves and friction modulation. Inspired by these characteristics, snail-like robots have recently become the focus of growing research. In this paper, we present a novel friction-driven three-foot snail-like robot which employs a simple mechanism to capture and replicate snail-like motion. This robot is driven by two servo motors, which makes it easy and low-cost to fabricate. The robot operates by breaking frictional symmetry in the cyclic motion of the three feet, in much the same way as the three-sphere Golestanian swimmer. The symmetry of its structure and properties of friction give the robot distinctive movements. We present a mathematical model of the robot's locomotion, focusing on its kinetic harmonic-peristaltic movement. We designed and fabricated the robot, then undertook simulations and experiments, which closely match the analytic solutions. This robot provides a new approach to realising simpler, lower cost, and potentially more efficient, biomimetic mobile robots.**

I. Introduction

Due to extraordinary moving ability, soft-body worms have become the focus of research to develop worm-like robots, mimicking, or partly mimicking, their movement. In the field of bioinspired worm-like robots, robots inspired by multi-foot worms such as caterpillars [1], [2] and inchworms [3] have been developed. Their feet act as anchors to improve stability, by which multi-foot movement [1] and omega-shape movement [3] can be replicated. Footless worms, in contrast, realise movement by travelling waves, inspiring robots designed to mimic earthworm [4] and gastropod [5] (hereafter called snail for clarity). Snails differ from other worm-like organisms because of relatively slow velocity and the mucus residue left on the substrate marking their path. However, snails are worthy of deep study due to their movement stability, load-carrying capability [5] and ability to locomote up vertical and along overhanging surfaces.

Snails exploit adhesive locomotion [6] through a unique movement mechanism, shown in Fig. 1 (a), which is the result of a balanced combination of friction forces [6], [7], suction forces [8], [9] and viscous forces [10]. In contrast to earthworms [11], snails generate contraction travelling waves from tail to head [6] as a result of muscular contraction-relaxation effects. Within a locomotion cycle, high and low pressures are generated, which cause mucus - a non-Newtonian fluid - to behave as a lubricant or as a solid [10], [12]. Both the rim of the snail and the solid mucus act to exert significant normal forces on substrate, so that a counter friction force drives the snail forward [6], [10], [12]. The snail rim also acts as seal such that the adhesive suction force is amplified by it. Snail adhesive locomotion is a complex interaction of compliant materials, multiphase fluids, body morphing and muscular actuation, which has not been fully replicated in a robot. However, some snail-like robots have been developed which partly mimic the snail's movement.

Chan *et al.* [5] developed two snail-like robots named Robosnail I and Robosnail II. They focused on mimicking retrograde and direct waves respectively, and successfully realised adhesive locomotion by applying an artificial mucus. Nakamura *et al.* [13], [14] developed a series of snail-like robots employing travelling waves and suction, which can move omnidirectionally on a spherical surface. In recent years snail-like robots have been developed with a range of actuation technologies, including motor-driven [5], [13]–[15], where researchers mainly focus on stable and efficient movement, and pneumatic [16]–[18], where softness is the first priority. They have been powered by novel energy sources, including light-driven [19] and natural-muscle-driven [20] mechanisms. Some are equipped with anchor-like magnetic adhesion [13], centrifugal fans [14] and SMA (Shape Memory Alloy) needles [15] to enhance stability. Despite these work, there has little study into how simple and fundamental actuation systems and robots can replicate snail like motion.

In this study, we present a novel three-foot robot to mimic the fundamental friction-driven movement of the snail. For clarity, the simplified schematic is shown in Fig. 1 (b). Three feet are actuated by two servo motors, causing reaction friction force to drive the robot forward.

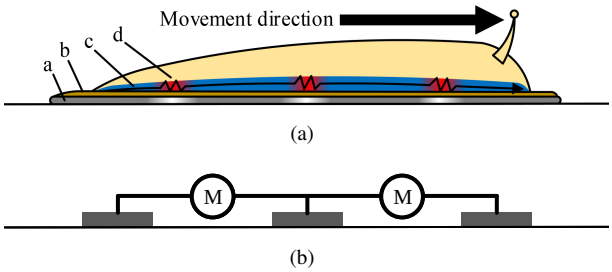

Fig. 1. (a) Schematic of how snails (shell ignored) move. a: mucus, where dark represents solid regions and light represents lubricating regions; b: rim; c: musculature and travelling wave, where red represents contraction and blue represents relaxation; d: snail's body. (b) Simplified schematic of the three-foot robot.

[1]Tianqi Yue, Hermes Bloomfield-Gadêlha and Jonathan Rossiter are with the Department of Engineering Mathematics and Bristol Robotics Laboratory at the University of Bristol, Bristol, BS8 1TR, UK {tianqi.yue, hermes.gadelha, jonathan.rossiter}@bristol.ac.uk

TY is funded by Chinese Scholarship Council through award 201906120027. JR was supported through EPSRC research grants EP/S026096/1, EP/R02961X/1 and EP/M020460/1, and by the Royal Academy of Engineering as a Chair in Emerging Technologies.

Unlike almost all prior snail-like robots, our robot employs no adhesion control. To study its fundamental behaviour, we constrain it to one degree of freedom. Bidirectional locomotion is achieved by breaking the symmetry of reactive friction forces generated by the three feet in response to lateral actuation forces. This symmetry-breaking behaviour is inspired by the three-sphere swimmer developed by Golestanian *et al.* [21], [22] where three identical spheres are made to 'swim' by imposing cycling forces between neighboring spheres, generating asymmetric drag forces. We extend this principle to land-based locomotion where friction is the dominant reactive force. In contrast to the Golestanian swimmer, where drag is a smooth function of velocity and surface areas, friction undergoes a threshold behaviour defined by the friction coefficient. Imbalance in friction forces is generated by breaking symmetry, which results in unique behaviours in our robot, and presents a challenge to develop the optimum actuating scheme for best locomotion. In this paper, we present the three-foot snail-like robot design, develop a mathematical model to explore kinetic properties and finally demonstrate its movement and compare simulations and experimental results with analytic solutions.

II. Design and Modeling

A. Three-foot Robot Design

The three-foot snail-like robot reduces actuation to its simplest form, operating over one degree of freedom. In this way we study the fundamental behaviour, and potential, of simple, potentially low-cost, gastropod robots. Fig. 2 presents a photo of the robot and a 3D rendered image. The middle foot (foot 2, green) is fixed on a linear guide, head (foot 3, blue) and tail (foot 1, red) feet are separately driven by two servo motors, by which foot 1 and foot 3 can slide along the linear guide with programmed velocity. The feet are made by laser cut acrylic sheet and white parts are fabricated by polylactic acid (PLA) 3D printing. The bottoms of all three feet are covered by sponge layers.

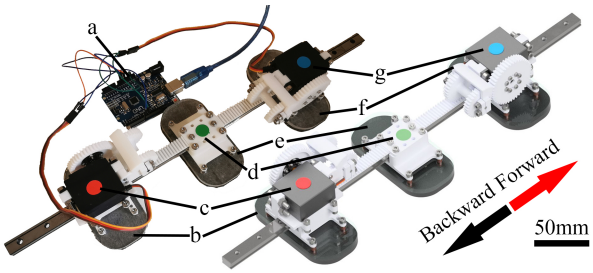

Fig. 2. a: Arduino® UNO board; b: foot 1 (tail foot); c: foot 1 servo motor; d: linear guide with gear rack; e: foot 2 (middle foot); f: foot 3 (head foot); g: foot 3 servo motor.

The dominant feature of this friction-driven model is the static friction threshold (i.e., limiting friction). We assume that the mass of the robot is always equally distributed on three feet and friction coefficients are identical for all feet. Foot displacement can only occur when the actuation force acting on a foot is bigger than the static friction threshold. This implies that the locomotion model is fundamentally different to models based on hydrodynamics (e.g., the Golestanian swimmer) or aerodynamics. The friction threshold acts to introduce a step response in the foot displacement function, causing discrete components in the mathematical model, which will be discussed in section III.

B. Movement Principle

In this study, we negate inertia effects and assume the robot moves with low acceleration. No external forces, beyond reactive friction, are applied on robot. With no inertia, at any time, at least one foot must be stationary. Let us name this the "stable movement" mode. Note that our model is displacement driven, as defined by the two servo motors, which are assumed to have sufficient force to overcome any friction threshold.

Let v_i be the relative velocity of foot i with respect to the substrate. The instantaneous velocity of the whole robot is represented by the mean translational velocity V, which is expressed as

$$V = \frac{1}{3}(v_1 + v_2 + v_3) \tag{1}$$

We assume that the servo motors are ideal - that is, they output self-adjusted velocity exactly matching their programming. The output of the servo motors are two relative velocities between three feet. Here we denote relative displacement between neighbouring foot i and foot $i+1$ as L_i, thus we know

$$\begin{aligned} \dot{L}_1 &= v_2 - v_1 \\ \dot{L}_2 &= v_3 - v_2 \end{aligned} \tag{2}$$

For stable movement, the robot always has at least one static foot as described above. Therefore, mean translational velocity V can be written in three forms

$$\begin{aligned} V|_{v_1=0} &= \frac{1}{3}(2\dot{L}_1 + \dot{L}_2) \quad \text{a)} \\ V|_{v_2=0} &= \frac{1}{3}(-\dot{L}_1 + \dot{L}_2) \quad \text{b)} \\ V|_{v_3=0} &= \frac{1}{3}(-\dot{L}_1 - 2\dot{L}_2) \quad \text{c)} \end{aligned} \tag{3}$$

We must determine which one, two or even three feet are static before selecting the velocity measure (i.e., determine the i where $v_i = 0$). As we assumed above, under low-acceleration inertial forces can be ignored, so the value of total kinetic friction F_k is equal to total static friction F_s. For this ideal case, we suppose static friction is equally distributed on all static feet. Under such simplified conditions, all possible classifications of static foot are listed below:

- If $\left\langle \hat{\dot{L}}_1, \hat{\dot{L}}_2 \right\rangle < 0$ and $\left|\dot{L}_1\right| < \left|\dot{L}_2\right|$, $v_1 = 0$.
- If $\left\langle \hat{\dot{L}}_1, \hat{\dot{L}}_2 \right\rangle \geq 0$, $v_2 = 0$.
- If $\left\langle \hat{\dot{L}}_1, \hat{\dot{L}}_2 \right\rangle < 0$ and $\left|\dot{L}_1\right| \geq \left|\dot{L}_2\right|$, $v_3 = 0$.

Based on the analysis above, we can calculate robot mean translational velocity through given $\dot{L}_1(t)$ and $\dot{L}_2(t)$.

III. Harmonic Movement

A. Pure Cosine Movement

Servo motors can output many types of movements, such as triangular, rectangular and harmonic waves. Normally, we want output acceleration to be continuous and smooth. For these reasons, harmonic movement is commonly used. Here we define the output of the two servo motors to be harmonic waves: $L_1(t) = A{\cdot}cos(\omega t){+}B$, $L_2(t) = A{\cdot}cos[\omega(t{-}\varphi)]{+}B$, where φ is the phase difference measured from L_1 to L_2, $\varphi \in [0, T)$. Fig. 3 illustrates how feet move in response to this actuation scheme. Here, for clarity, we fix the reference frame on foot 2 and let $\varphi = T/4$, to show how feet move relative to robot center in harmonic movement.

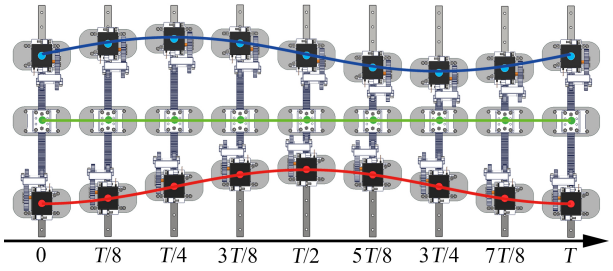

Fig. 3. Illustration of how feet move in response to harmonic actuation, $\varphi = T/4$. Red line: foot 1; green line: foot 2; blue line: foot 3. Reference frame is fixed on the center of foot 2.

Based on analysis in section II.B, the classification of static and moving feet is with definite relation to $\dot{L}_1$ and $\dot{L}_2$. We now combine harmonic (cosine) expressions with the former analysis of foot classification, to determine the expected movement of each foot. Then we get,

if $\varphi \in [0, T/2)$,

$$\begin{cases} t \in \left[0, \frac{\varphi}{2}\right) \cup \left[\frac{T}{2}, \frac{T}{2} + \frac{\varphi}{2}\right) & v_1 = 0 \\ t \in \left[\varphi, \frac{T}{2}\right) \cup \left[\frac{T}{2} + \varphi, T\right) & v_2 = 0 \\ t \in \left[\frac{\varphi}{2}, \varphi\right) \cup \left[\frac{T}{2} + \frac{\varphi}{2}, \frac{T}{2} + \varphi\right) & v_3 = 0 \end{cases}$$

if $\varphi \in [T/2, T)$,

$$\begin{cases} t \in \left[\frac{\varphi}{2}, \frac{T}{2}\right) \cup \left[\frac{T}{2} + \frac{\varphi}{2}, T\right) & v_1 = 0 \\ t \in \left[0, \varphi - \frac{T}{2}\right) \cup \left[\frac{T}{2}, \varphi\right) & v_2 = 0 \\ t \in \left[\varphi - \frac{T}{2}, \frac{\varphi}{2}\right) \cup \left[\varphi, \frac{T}{2} + \frac{\varphi}{2}\right) & v_3 = 0 \end{cases}$$

We find that these intervals are divided into two parts, implying that every foot has two separated "static intervals" in one period. We also observed that intervals are periodic, with period equal to $T/2$. It is straightforward to obtain the equation of individual foot movement with respect to substrate in form of $k_1 \cdot sin(\omega t) + k_2 \cdot sin[\omega(t - \varphi)]$, where k_1 and k_2 are constants.

Here we discuss the average velocity V_a, which is given by $V_a = D_{net}/T$ where D_{net} is the net displacement over $[0, T)$. This quantity shows how the cosine wave affects robot movement. Substituting in cosine movement expressions we find that V_a only consists of constant terms, $k \cdot cos(\omega\varphi)$ and $k \cdot cos(\omega\varphi/2)$, and the sum of these terms are 0.

$$V_a = 0 \quad \varphi \in [0, T) \tag{4}$$

Equation (4) implies that a pure cosine actuation scheme does not cause robot movement, no matter what phase difference φ is chosen. To further verify this effect, we substitute $t_2 = t_1 + T/2$ to obtain,

$$\begin{aligned} v_i|_{t_1} &= k_1 \cdot sin\left(\omega t_1\right) + k_2 \cdot sin\left[\omega\left(t_1 - \varphi\right)\right] \\ &= -v_i|_{t_2} = -\{k_1 \cdot sin\left(\omega t_2\right) + k_2 \cdot sin\left[\omega\left(t_2 - \varphi\right)\right]\} \end{aligned} \tag{5}$$

Equation (5) implies that all feet undergo an opposite movement to their previous movement at time $T/2$ ago. Therefore, after one cycle, all feet return back to their initial positions and initial velocities. To illustrate this more clearly, Fig. 4 shows the free movement of each foot of the robot over a complete cycle. Note that the state and position of the robot at time T is identical to time 0, implying that $V_a = 0$ is not a function of φ.

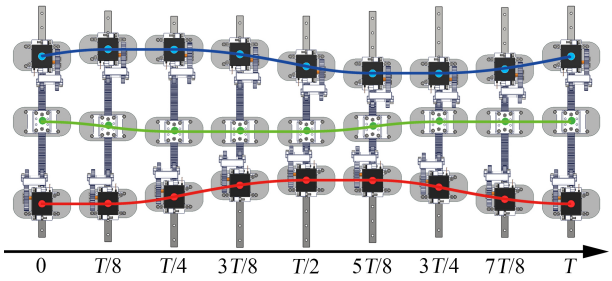

Fig. 4. Illustration of robot movement, relative to world reference frame, $\varphi = T/4$. Over one cycle, net displacement is 0.

B. Cosine-line Movement

Above, we proved that harmonic actuation cannot generate net motion of a three-foot friction-driven robot, regardless of the phase of the two actuators. We now present the concept of generating non-zero net displacement by breaking the symmetry of this system. This can be achieved through two routes: 1. Break structural symmetry - introduce friction anisotropy, for example by adding directional friction coatings (e.g., micro hairs mimicking worm setae) to the feet, or 2. Break actuation symmetry - introduce asymmetry to servo drive signals. Here we choose the latter one.

In many animals, locomotion is achieved by the repeated movement on one limb when the other limbs are stationary. Similarly, we introduce a modification to the harmonic actuation function above. A $T/2$ long segment, during which the actuator does not move, is added to the end of cosine

wave, where T is the period of former cosine wave. By this we obtain a combined cosine-line wave with period $3T/2$.

By the same approach discussed in pure cosine actuation, individual foot movement can be divided into discrete intervals, determined by phase difference φ, i.e., $\varphi \in [0, T/2)$, $\varphi \in [T/2, T)$ and $\varphi \in [T, 3T/2)$. Equations of these intervals have similar form to pure cosine movement, and we do not include them here for brevity.

In contrast to pure cosine movement, the symmetry of a cosine wave is broken by adding a line segment. Therefore, individual foot velocities are still periodic but net displacement D_{net} over $[0, 3T/2)$ is non-zero. The value of average velocity V_a is given by $V_a = 2D_{net}/(3T)$

$$V_a = \begin{cases} \frac{4A}{3T}\left[1 - cos\left(\frac{\omega\varphi}{2}\right)\right] & \varphi \in \left[0, \frac{T}{2}\right) \\ \frac{4\sqrt{2}A}{3T} sin\left(\frac{\omega\varphi}{2} + \frac{\pi}{4}\right) & \varphi \in \left[\frac{T}{2}, T\right) \\ -\frac{4A}{3T}\left[sin\left(\frac{\omega\varphi}{2}\right) + 1\right] & \varphi \in \left[T, \frac{3T}{2}\right) \end{cases}$$

When $\varphi = T/2$, the robot has maximum average forward velocity V_{a_max}, and when $\varphi = T$, the robot has maximum backward velocity $-V_{a\_max}$. As an example, the schematic of movement driven by cosine-line actuation when $\varphi = T/2$ is shown in Fig. 5. In this case, no backward slippage is observed, and thus forward velocity is maximum. Retrograde slippage of feet, and hence reduction in forward motion, occurs for other values of φ.

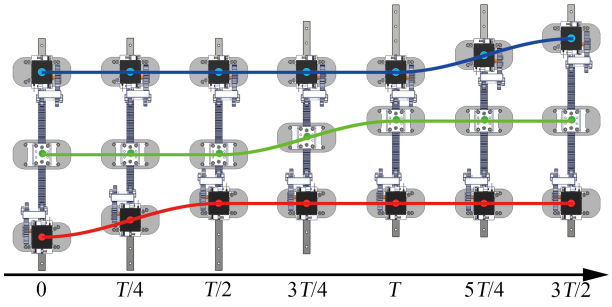

Fig. 5. Schematic illustrating how feet move under cosine-line actuation for optimum $\varphi = T/2$. No backward slippage occurs and one foot is always moving forward while the other two are stationary.

Since for cosine-line movement, robot average velocity is no longer zero but a function of phase difference, we can now consider power consumption. In this model we ignore the static-kinetic friction transition stage so that system energy loss in one cycle equals the total work done against kinetic friction. Average power P_a is given by,

$$P_a = \begin{cases} \frac{4Af_k}{3T}\left[3 + cos\left(\frac{\omega\varphi}{2}\right)\right] & \varphi \in \left[0, \frac{T}{2}\right) \\ \frac{4\sqrt{2}Af_k}{3T}\left[\sqrt{2} + sin\left(\frac{\omega\varphi}{2} - \frac{\pi}{4}\right)\right] & \varphi \in \left[\frac{T}{2}, T\right) \\ \frac{4Af_k}{3T}\left[3 - sin\left(\frac{\omega\varphi}{2}\right)\right] & \varphi \in \left[T, \frac{3T}{2}\right) \end{cases}$$

Where f_k is the kinetic friction applied on individual foot. Clearly, the average power P_a is also a function of phase difference φ.

We show average velocity V_a and average power P_a as a polar plot in Fig. 6 to show how they vary with respect to φ, from 0 to $3T/2$. It is clear that we can modify movement direction and velocity (V_a) simply by changing φ if the robot is actuated by a cosine-line wave. P_a is symmetric to the horizontal intersect $[3T/4, 3T/2]$, and is minimum at $\varphi = T/2$ and $\varphi = T$, where V_a is also maximum in two directions. Therefore, the robot will locomote with the highest speed and highest efficiency when $\varphi = T/2$ (forward) or $\varphi = T$ (backward).

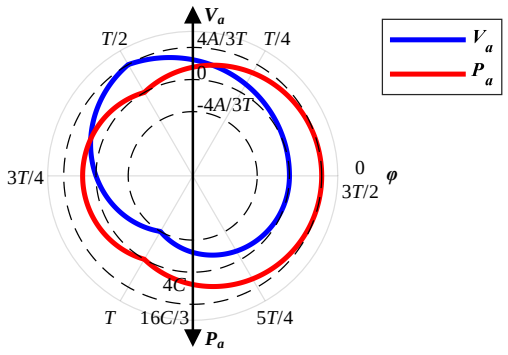

Fig. 6. Average velocity V_a and average power P_a as function of phase difference φ, in cosine-line movement. $C = Af_k/T$.

IV. Simulations and Experiments

Simulations were implemented on MATLAB® Simscape Multibody™. We used the embedded Spatial Contact Force block to simulate friction. Note that this block models the small-scale mechanical interactions that result in observable friction, and tends to introduce small variations in the macro friction behaviour. Even so, we can have high confidence in the overall behaviours shown by the simulation since the simulation results is extremely close to analytic solution. Experiments with the physical robot were carried out on a flat varnished wood substrate.

A. Foot Trajectory Verification

The servo motor actuation functions used in simulations and experiments are presented in Tab. I. Fig. 7 and Fig. 8 show results of pure cosine movement and cosine-line movement, respectively.

TABLE I
Actuation function

Movement	Actuation function
Pure cosine (mm)	$L_1 = 29cos(\frac{2\pi}{T}t) + 113$
	$L_2 = 29cos[\frac{2\pi}{T}(t-\varphi)] + 113$
Cosine-line (mm)	$L_1 = 29cos(\frac{2\pi}{T}t) + 113 \quad t \in [0, T)$
	$L_1 = 142 \quad t \in [T, \frac{3T}{2})$
	$L_2 = 29cos[\frac{2\pi}{T}(t-\varphi)] + 113 \quad t \in [\varphi, \varphi + T)$
	$L_2 = 142 \quad t \in [0, \varphi) \cup [\varphi + T, \frac{3T}{2})$

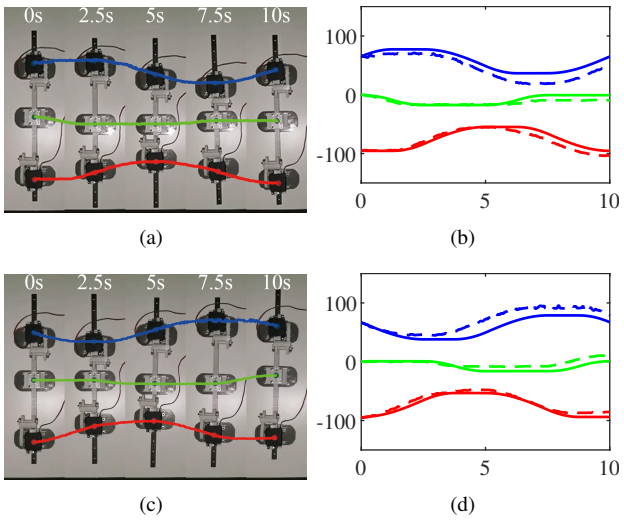

Fig. 7. Pure cosine movement simulation and experimental results. x axis label: time (s); y axis label: foot displacement (mm). Red line: foot 1; green line: foot 2; blue line: foot 3. (a) $\varphi = T/4$, experimental snapshots of robot position and motion. (b) $\varphi = T/4$, comparison between simulation (solid) and experimental results (dashed lines). (c) $\varphi = 3T/4$, experimental snapshots of robot position and motion. (d) $\varphi = 3T/4$, comparison between simulation and experimental results.

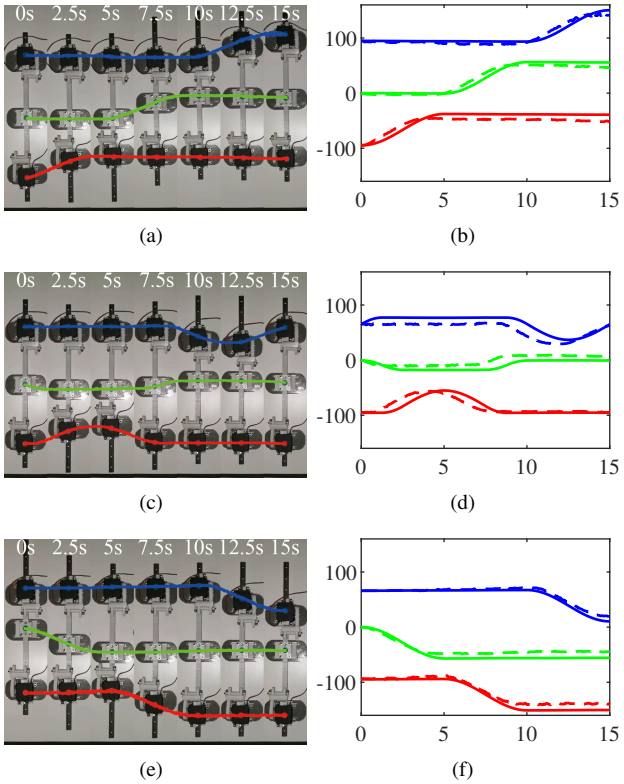

Fig. 8. Cosine-line movement simulation and experimental results. x axis label: time (s); y axis label: foot displacement (mm). (a) $\varphi = T/2$, experimental snapshots of robot position and motion. (b) $\varphi = T/2$, comparison between simulation (solid) and experimental results (dashed lines). (c) $\varphi = 3T/4$, experimental snapshots of robot position and motion. (d) $\varphi = 3T/4$, comparison between simulation and experimental results. (e) $\varphi = T$, experimental snapshots of robot position and motion. (f) $\varphi = T$, comparison between simulation and experimental results.

We chose $\varphi = T/4$ and $\varphi = 3T/4$ to verify pure cosine movement, while $\varphi = T/2$, $\varphi = 3T/4$ and $\varphi = T$ are selected to verify cosine-line movement. These values lead to more illustrative results, with more direction changes than that of $\varphi = 0$ and $\varphi = T/2$ in pure cosine wave or $\varphi = 0$ in cosine-line movement. Simulation and experimental results are plotted together for comparison. Analytical results were extremely close to simulation results so are omitted for clarity.

For pure cosine movement (Fig. 7), as predicted when $\varphi = T/4$ and $\varphi = 3T/4$, the robot undergoes symmetrical movement. All feet return back to their initial positions after one period, demonstrating that robot has zero average velocity V_a in pure cosine movement.

For cosine-line movement (Fig. 8), results are also consistent with simulations (and the analytic solution). When $\varphi = T/2$, the robot undergoes maximum forward movement, and at $\varphi = T$, the robot undergoes maximum backward movement. When $\varphi = 3T/4$ (center of period), the robot has zero average velocity. Experiments and simulations successfully demonstrated that cosine-line actuation results in robot locomotion, and this motion (and power efficiency) is controllable by adjusting phase difference φ.

Experimental results show small deviation from simulation results (and the analytic solution), especially for pure cosine movement. That is caused by slight backward slippage of some feet, which was observed during experiments and is shown in the supplementary video. Possible causes include: servo motor control jitter which makes robot 'tremble', causing sudden high acceleration and momentary exceeding of friction threshold; contacting surfaces have static-kinetic friction transition stage which is ignored in the analysis; bottom surfaces of the robot's feet are not strictly on the same plane or the substrate is not strictly flat; or gaps between gears and rack cause gear chatter. Overall, experimental results of foot trajectories closely match the analytic solution and simulation results.

B. Average Velocity Verification

Further experiments were carried out to verify average velocity for different phase differences φ, with results shown in Fig. 9. We chose 9 equidistant phase values for pure cosine movement and 13 equidistant values for cosine-line movement across the actuation period, actuated by two periods, 10 seconds and 5 seconds and wave functions are the same as Tab. I. We compared experimental results with both simulation results and the analytic solution. For clarity, we normalized the x (time) axis while making no change to the y (displacement) axis.

Fig. 9 shows that simulation results match the analytical model very well. Experimental results are very close to the analytic solution but show small deviation, which is due to the slight backward slippage discussed above. Overall, foot trajectory and average velocity both show good consistency between analysis, simulations and experiments. These results show the veracity of the model and the potential of this novel robot.

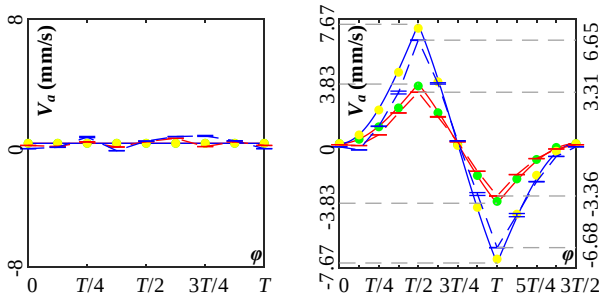

Fig. 9. Robot average velocity with respect to phase difference. (a) Pure cosine movement. (b) Cosine-line movement. Red line: analytic solution (overlapped by blue line in (a)), $T = 10$s. Blue line: analytic solution, $T = 5$s. Green dots: simulation results (overlapped by yellow dots in (a)), $T = 10$s. Yellow dots: simulation results, $T = 5$s. Red dashed line: experimental results, $T = 10$s. Blue dashed line: experimental results, $T = 5$s.

V. Conclusions

Inspired by snail movement, we presented a novel friction-driven three-foot robot. Actuated by two servo motors, the robot moves bidirectionally (forward and backward) by breaking the symmetry of friction reaction forces. We presented a simplified mathematical model and explored the kinetics properties of this robot, then applied harmonic movement to drive it. We focused on the parameters of harmonic movement, and the effects of phase difference between the two servo motors' driving signals. We found that when driven by pure cosine actuation, the robot's average velocity always equals zero, regardless of the phase difference. In contrast, when driven by a cosine-line actuation, the robot can move with non-zero average velocity, and the average velocity can be programmed by changing phase difference. Under cosine-line actuation, maximum average velocity in both forward and backward directions can be realised by choosing the optimum phase difference, $\varphi = T/2$ and $\varphi = T$ respectively. We carried out simulations and experiments to verify the model presented, with results matching the analytic solution well.

This robot has a simple and symmetrical structure, and yet it can move by breaking its intrinsic symmetry. The robot is purely driven by friction, which may provide a novel solution for future friction-driven mobile robots. The friction threshold plays an important role on the robot's locomotion, makes it stable and easy to control. Moreover, the three-foot robot presented here has good extensibility: it can be further combined with anchor mechanisms to move efficiently over terrain with varying friction; and acceleration feedback can be used to control in the presence of inertia, thereby increasing robot speed. These will be the focus of future work. This study provides a new path to realise novel friction-driven movements which can be exploited in many fields, from biomimetics to mobile robotics.

References

[1] H.-T. Lin, G. G. Leisk, and B. Trimmer, "Goqbot: a caterpillar-inspired soft-bodied rolling robot," *Bioinspiration & biomimetics*, vol. 6, no. 2, p. 026007, 2011.

[2] X. Huang, K. Kumar, M. K. Jawed, A. M. Nasab, Z. Ye, W. Shan, and C. Majidi, "Chasing biomimetic locomotion speeds: Creating untethered soft robots with shape memory alloy actuators," *Science Robotics*, vol. 3, no. 25, p. eaau7557, 2018.

[3] J.-S. Koh and K.-J. Cho, "Omegabot: Biomimetic inchworm robot using sma coil actuator and smart composite microstructures (scm)," in *2009 IEEE International Conference on Robotics and Biomimetics (ROBIO)*. IEEE, 2009, pp. 1154–1159.

[4] S. Seok, C. D. Onal, R. Wood, D. Rus, and S. Kim, "Peristaltic locomotion with antagonistic actuators in soft robotics," in *2010 IEEE International Conference on Robotics and Automation*. IEEE, 2010, pp. 1228–1233.

[5] B. Chan, N. Balmforth, and A. Hosoi, "Building a better snail: Lubrication and adhesive locomotion," *Physics of fluids*, vol. 17, no. 11, p. 113101, 2005.

[6] J. H. Lai, J. C. del Alamo, J. Rodríguez-Rodríguez, and J. C. Lasheras, "The mechanics of the adhesive locomotion of terrestrial gastropods," *Journal of Experimental Biology*, vol. 213, no. 22, pp. 3920–3933, 2010.

[7] M. W. Denny, "A quantitative model for the adhesive locomotion of the terrestrial slug, ariolimax columbianus," *Journal of experimental Biology*, vol. 91, no. 1, pp. 195–217, 1981.

[8] A. M. Smith, "The role of suction in the adhesion of limpets," *Journal of Experimental Biology*, vol. 161, no. 1, pp. 151–169, 1991.

[9] K.-I. Kim, Y.-T. Kim, and D.-E. Kim, "Adhesion characteristics of the snail foot under various surface conditions," *International Journal of Precision Engineering and Manufacturing*, vol. 11, no. 4, pp. 623–628, 2010.

[10] R. H. Ewoldt, C. Clasen, A. E. Hosoi, and G. H. McKinley, "Rheological fingerprinting of gastropod pedal mucus and synthetic complex fluids for biomimicking adhesive locomotion," *Soft Matter*, vol. 3, no. 5, pp. 634–643, 2007.

[11] N. Saga and T. Nakamura, "Development of a peristaltic crawling robot using magnetic fluid on the basis of the locomotion mechanism of the earthworm," *Smart materials and structures*, vol. 13, no. 3, p. 566, 2004.

[12] M. Denny, "The role of gastropod pedal mucus in locomotion," *Nature*, vol. 285, no. 5761, pp. 160–161, 1980.

[13] T. Go, T. Osawa, and T. Nakamura, "Proposed locomotion strategy for a traveling-wave-type omnidirectional wall-climbing robot for spherical surfaces," in *2015 IEEE International Conference on Robotics and Biomimetics (ROBIO)*. IEEE, 2015, pp. 2223–2228.

[14] T. Yamaguchi, T. A. Tetsuhide Go, Y. Yamada, and T. Nakamura, "Development of negative pressure suction mechanism in omnidirectional wall-climbing robot for inspection of airplanes," in *Advances in Cooperative Robotics*. World Scientific, 2017, pp. 106–114.

[15] M. Watanabe and H. Tsukagoshi, "Snail inspired climbing robot using fluid adhesion to travel on rough concrete walls and ceilings," in *Advances in Cooperative Robotics*. World Scientific, 2017, pp. 79–87.

[16] ——, "Soft sheet actuator generating traveling waves inspired by gastropod's locomotion," in *2017 IEEE International Conference on Robotics and Automation (ICRA)*. IEEE, 2017, pp. 602–607.

[17] J. Takeyama, A. Ichikawa, A. Hasegawa, E. Kim, and T. Fukuda, "A soft robot mimicking snail's foot," in *2018 International Symposium on Micro-NanoMechatronics and Human Science (MHS)*. IEEE, 2018, pp. 1–3.

[18] J. Chan, F. T. Pan, and Z. Li, "Design and motion control of biomimetic soft crawling robot for gi tract inspection," in *2018 13th World Congress on Intelligent Control and Automation (WCICA)*. IEEE, 2018, pp. 1366–1369.

[19] M. Rogóż, K. Dradrach, C. Xuan, and P. Wasylczyk, "A millimeter-scale snail robot based on a light-powered liquid crystal elastomer continuous actuator," *Macromolecular rapid communications*, vol. 40, no. 16, p. 1900279, 2019.

[20] M. U. Akhtar, L. Gao, H. Wen, Q. Gao, B. Zhang, Q. Lian, and D. Li, "Design of a biohybrid robot by mimicking the gait mechanism of aplysia californica," *Procedia CIRP*, vol. 89, pp. 154–158, 2020.

[21] R. Golestanian and A. Ajdari, "Analytic results for the three-sphere swimmer at low reynolds number," *Physical Review E*, vol. 77, no. 3, p. 036308, 2008.

[22] A. Najafi and R. Golestanian, "Simple swimmer at low reynolds number: Three linked spheres," *Physical Review E*, vol. 69, no. 6, p. 062901, 2004.